nature chemical biology

ARTICLE

PUBLISHED ONLINE: 26 OCTOBER 2014 | DOI: 10.1038/NCHEMBIO.1661

Hydrolysis of 2′3′-cGAMP by ENPP1 and design of nonhydrolyzable analogs

Lingyin Li[1]*, Qian Yin[2], Pia Kuss[3], Zoltan Maliga[1], José L Millán[3], Hao Wu[2] & Timothy J Mitchison[1]

Agonists of mouse STING (TMEM173) shrink and even cure solid tumors by activating innate immunity; human STING (hSTING) agonists are needed to test this therapeutic hypothesis in humans. The endogenous STING agonist is 2′3′-cGAMP, a second messenger that signals the presence of cytosolic double-stranded DNA. We report activity-guided partial purification and identification of ecto-nucleotide pyrophosphatase/phosphodiesterase (ENPP1) to be the dominant 2′3′-cGAMP hydrolyzing activity in cultured cells. The hydrolysis activity of ENPP1 was confirmed using recombinant protein and was depleted in tissue extracts and plasma from *Enpp1*$^{-/-}$ mice. We synthesized a hydrolysis-resistant bisphosphothioate analog of 2′3′-cGAMP (2′3′-cG^{s}A^{s}MP) that has similar affinity for hSTING *in vitro* and is ten times more potent at inducing IFN-β secretion from human THP1 monocytes. Studies in mouse *Enpp1*$^{-/-}$ lung fibroblasts indicate that resistance to hydrolysis contributes substantially to its higher potency. 2′3′-cG^{s}A^{s}MP is therefore improved over natural 2′3′-cGAMP as a model agonist and has potential as a vaccine adjuvant and cancer therapeutic.

Activation of innate immune signaling is a proven therapeutic strategy in vaccination[1,2], viral infection[3] and cancer (for example, BCG for bladder cancer and imiquimod for skin cancer). Vaccine adjuvants and immune-activating anticancer agents have traditionally depended on relatively broad or nonspecific stimuli, such as attenuated or killed bacteria or alum crystals. An improved understanding of innate immune signaling should make it possible to design more precise immunostimulants for treating or preventing specific diseases. The discovery of the STING pathway, a central pathway in antiviral innate immunity[4,5], and the second messenger cyclic dinucleotides (CDNs) that activate it[6] opened up several new possibilities in this area. STING agonists would be candidates for clinical testing as adjuvants and as stimulants for anticancer immune activity. We and others recently found that DMXAA, which markedly shrinks cancer in mouse model systems by activating the innate immune response, is a STING agonist that activates mouse STING (mSTING) but not hSTING[7–9]. To test the therapeutic hypothesis that STING agonists will be effective for cancer treatment and/or as vaccine adjuvants, we need molecules that are active in humans. The most potent natural STING agonist in humans is 2′3′-cGAMP (**2**). We set out to identify a stable agonist for hSTING. To do this, we first investigated the major degradation mechanism of 2′3′-cGAMP and then constructed 2′3′-cGAMP analogs that are resistant to its activity.

STING is an endoplasmic reticulum (ER) transmembrane protein. The cytoplasmic domain of STING forms dimers, and CDNs bind at the dimer interface[10]. Upon ligand binding, the cytoplasmic tail of STING serves as an adaptor for TBK-1 (a kinase) and IRF-3 (a transcription factor), resulting in their phosphorylation[11]. Phosphorylated IRF-3 translocates into the nucleus to induce a panel of host response genes, including those encoding interferon α and β. In bacterial infection, STING is activated by conserved bacterial second messengers, cyclic dinucleotides linked through two 3′-5′ phosphodiester linkages (3′3′-CDNs), which can contain two guanosines, two adenosines or one of each[12]. A second more powerful activation signal results from the presence of viral or self double-stranded DNA (dsDNA) in the cytoplasm, leading to the synthesis of 2′3′-cGAMP, which is a heterodimer linked by one standard 3′-5′ phosphodiester and one rare 2′-5′ phosphodiester[13–15]. The affinity of 2′3′-cGAMP for hSTING is very high, with a dissociation constant of 4.59 nM compared to >1 μM for bacterial 3′3′-CDNs.

CDNs do not resemble typical small-molecule drug candidates. Their molecular weight is ~700 Da, they have two negative charges, and they are built from potentially labile phosphodiester linkages. Nevertheless, they are able to activate the STING pathway, presumably after entering the cell by unknown mechanisms[9]. Moreover, 2′3′-cGAMP has shown potential as an immune adjuvant in mouse studies[16]. These observations and its high affinity to hSTING suggest that molecules directly based on 2′3′-cGAMP have therapeutic potential. However, important questions remain, including the hydrolytic stability of CDN derivatives in the circulation and tissues.

Other second messengers containing phosphodiester linkages are rapidly hydrolyzed by specific enzymes, and in some cases the hydrolytic enzymes are important drug targets. For example, cAMP and cGMP are degraded by 11 classes of phosphodiesterases (PDEs), and PDE5 is the target of Viagra[17,18]. Intracellular cAMP and cGMP are also exported from the cell by ATPase pumps: ABCC4 (alternatively named MRP4)[19], ABCC5 (MRP5)[20] and ABCC11 (MRP8)[21] have all been implicated in cyclic nucleotide export. No degradation or export pathways for 2′3′-cGAMP are known. Here, we describe the identification of ENPP1 as the dominant 2′3′-cGAMP hydrolase in cells, tissue extracts and blood. We also report hydrolysis-resistant CDN analogs that retain strong hSTING agonist activity.

RESULTS

PDE12 does not hydrolyze 2′3′-cGAMP

We enzymatically synthesized 2′3′-cGAMP from GTP and ATP using the mouse cyclic-GMP-AMP synthase (cGAS) construct[22,23] and 3′3′-cGAMP (**1**) using DncV from *Vibrio cholerae*[12]. ^{32}P-labeled versions were synthesized by including trace [α-^{32}P]ATP. Synthesis and hydrolysis of radiolabeled CDNs were assayed using a simple

[1]Department of Systems Biology, Harvard Medical School, Boston, Massachusetts, USA. [2]Program in Cellular and Molecular Medicine, Boston Children's Hospital, Boston, Massachusetts, USA. [3]Sanford Children's Health Research Center, Sanford-Burnham Medical Research Institute, La Jolla, California, USA. *e-mail: lingyin_li@hms.harvard.edu

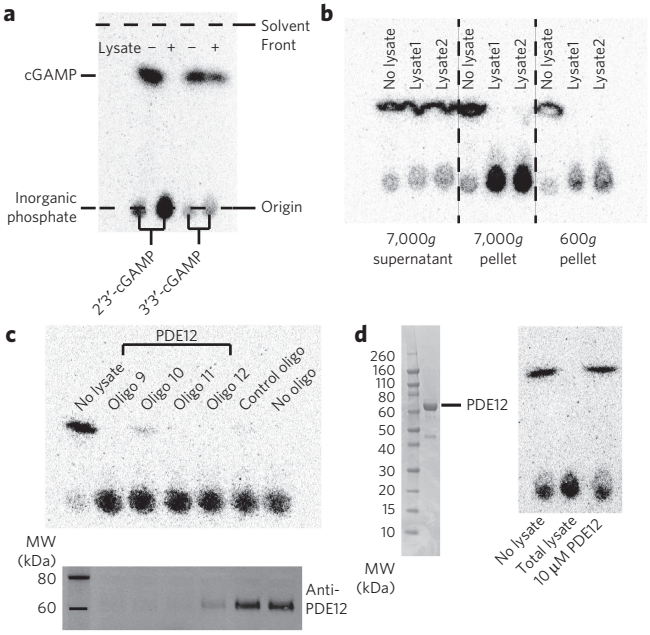

Figure 1 | There is 2′-5′ phosphodiesterase activity in the plasma membrane or heavy organelles and it is not due to PDE12. (**a**) 2′3′-cGAMP and 3′3′-cGAMP hydrolysis reactions. THP-1 cells were lysed using 1% NP-40. The ^{32}P-labeled CDNs were incubated with the cell lysate for 20 h, and the reaction was monitored using a TLC assay and visualized by autoradiography. (**b**) 2′3′-cGAMP hydrolase activity in differential centrifugation fractions of MDA-MB231 cells. Cells were suspended in isotonic buffer and lysed with a Dounce homogenizer. Supernatant and pellets from spins at the indicated speeds were solubilized and assayed in 1% NP-40, 20 mM Tris-HCl, pH 7.5, and 1 mM Ca^{2+}. (**c**) Knockdown of PDE12 does not decrease hydrolase activity. MDA-MB231 cells were transfected with four siRNA oligos against PDE12 and a control oligo. After 4 d, cells were lysed in the same buffer as in **b** and assayed for activity. Top, hydrolase activity in cells treated with different siRNA oligos. Bottom, PDE12 levels in these cells. MW, molecular weight. (**d**) Activity of purified PDE12 compared with that of MDA-MB231 whole-cell lysate.

thin-layer chromatography (TLC) assay (**Fig. 1a**). The TLC assay separates small molecules by their polarity, with less polar compounds migrating higher on the plate. We chose a solvent condition that moves CDNs up while leaving ATP and GTP and the final hydrolysis product, inorganic phosphate, at the baseline. Using this assay, we first searched for hydrolase activities in cell lines. We used mouse L929 cells and human THP-1 cells, both of which are model cell lines for the STING pathway and are capable of synthesizing 2′3′-cGAMP (**2**) in response to dsDNA[23]. By fractioning cells by differential centrifugation, we discovered that the cytosol from these cells contained negligible activity. Detergent (NP-40) extracts of the cells had much higher activity, suggesting that the activity is located in an organelle or on the plasma membrane (**Supplementary Results**, **Supplementary Fig. 1a**). We invested considerable effort investigating buffer conditions and found that Ca^{2+} was required for hydrolase activity and that both EDTA and EGTA abolished activity (**Supplementary Fig. 1b**). Resting cytosolic Ca^{2+} level is in the nanomolar range and can only go up to micromolar range transiently, so this observation again suggested that the activity is unlikely to reside in the cytosol. 2′3′-cGAMP was degraded much faster than 3′3′-cGAMP, suggesting that the predominant, Ca^{2+}-requiring hydrolase may prefer the 2′-5′ phosphodiester bond (**Fig. 1a**).

Although there are 11 classes of phosphodiesterases (PDE1–PDE11) that degrade the 3′-5′ phosphodiester bond in cAMP and cGMP, these PDEs are not thought to degrade 2′-5′ phosphodiesters. Only PDE12 is known to hydrolyze a 2′-5′ phosphodiester bond[24]. In addition, PDE12 resides in the matrix of mitochondria, consistent with the organelle- or membrane-bound hydrolase activity we observed[25]. We therefore tested the hypothesis that PDE12 might account for the hydrolase activity in detergent extracts of MDA-MB231 cells, a metastatic breast cancer cell line that expresses high levels of PDE12. We performed differential centrifugation on MDA-MB231 cells and, again, no activity was observed in the cytosol, but it was observed in the pellet resulting after centrifugation at 7,000*g*, indicative of heavy membranes or heavy organelles (**Fig. 1b**). We dissolved the pellet in NP-40 and performed column fractionation. The activity of the fractions indicates that there is one dominant hydrolase (**Supplementary Fig. 2**). To test whether this activity is due to PDE12, we blotted these fractions using a PDE12 antibody (**Supplementary Fig. 2**). Unambiguously, active fractions and fractions containing PDE12 do not overlap, suggesting that PDE12 does not account for the major hydrolase activity. We further confirmed this conclusion by knocking down PDE12 in these cells. All four siRNA sequences effectively knocked down PDE12 on the protein level but had no effect on the hydrolase activity in the cell lysate (**Fig. 1c**). Using purified PDE12 protein, we showed that it does not have activity toward 2′3′-cGAMP at concentrations much higher than its physiological concentration (**Fig. 1d**). Together, our results demonstrated that even though the hydrolase activity localizes in heavy membranes or organelles, it is not from PDE12.

ENPP1 is the dominant 2′3′-cGAMP hydrolase

We next sought a bulk tissue source to purify and identify the hydrolase. Liver is a classic source for organelle and enzyme purification. We detected high activity in mouse livers, again in the 7,000*g* pellet (**Supplementary Fig. 3a**). Because a calf liver provides more starting material, we performed differential centrifugation followed by detergent solubilization, anion exchange fractionation and size exclusion fractionation on calf liver extract (**Supplementary Fig. 3b–h**). Fraction 26 from the last purification step has a low protein concentration that is undetectable by SDS-PAGE gel but has high hydrolytic activity. MS analysis of this fraction revealed 377 proteins, and a top-ranking protein, ENPP1, appeared to be the most plausible candidate (**Supplementary Data Set**)[26,27]. ENPP1 is a plasma membrane and ER lumen protein[28], which agrees with our cell fractionation results. In addition, the structure of ENPP1 revealed that it has a Ca^{2+}-binding domain and chelates two Zn^{2+} ions in the catalytic site[29]. Consistent with the ion dependency of ENPP1, addition of Ca^{2+} and Zn^{2+} both boosted the hydrolase activity in the active fractions (**Fig. 2a** and **Supplementary Fig. 4a**). Moreover, we found the optimal pH for the liver hydrolase activity to be 9.0, which agrees with that of ENPP1 (**Fig. 2b** and **Supplementary Fig. 4b**). We noticed that 2′3′-cGAMP migrates differently at pH 6.5 and 7.0 compared to other pH conditions. This is due to the changed polarity of 2′3′-cGAMP at these conditions rather than its hydrolysis state because the same shift can be observed without lysate (**Supplementary Fig. 5a**). Nevertheless, 2′3′-cGAMP and the hydrolysis product at the baseline are well separated in all conditions. Finally, recombinant ENPP1 at nanomolar concentrations efficiently degraded 2′3′-cGAMP (**Fig. 2c**). The degradation product migrates together with AMP in TLC experiments. Addition of alkaline phosphatase converted the product to inorganic phosphate, showing that no phosphodiester bonds remained after ENPP1 action (**Fig. 2d**). Together, our results suggest that ENPP1 accounts for the observed hydrolase activity.

ENPP1 has high 2′-3′ cGAMP hydrolase activity

The best-characterized substrate of ENPP1 is ATP, which is hydrolyzed to AMP and PPi[29]. We compared the activity of ENPP1 toward 2′3′-cGAMP and ATP. Kinetic analysis showed that ENPP1 efficiently hydrolyzes both ATP (K_{cat} = 12 s^{-1}, K_m = 20 μM) and

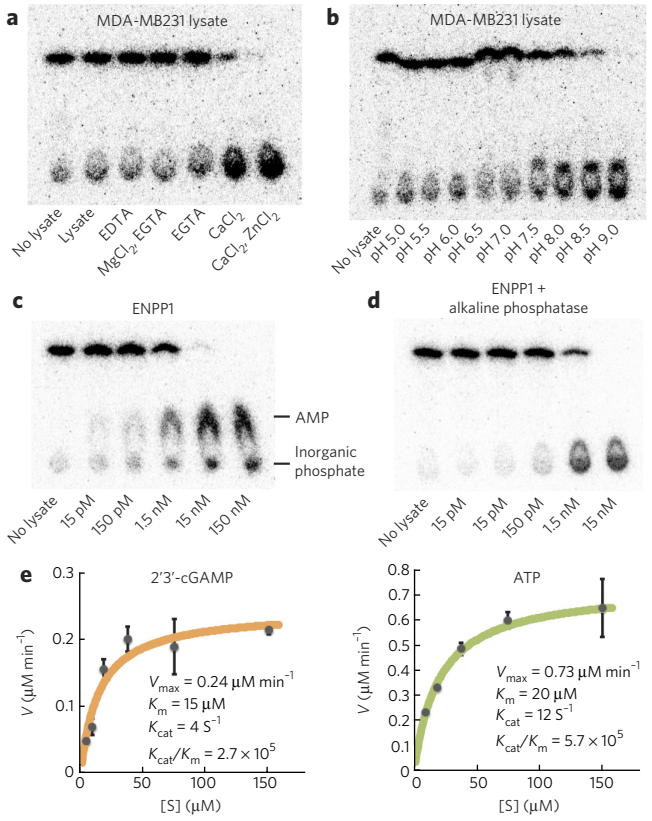

Figure 2 | ENPP1 is an efficient hydrolase for 2′3′-cGAMP. (**a**,**b**) Ion dependency (**a**) and pH preference (**b**) of the dominant hydrolase activity in MDA-MB231 cells. (**c**,**d**) Activity of recombinant ENPP1 alone (**c**) or coupled to alkaline phosphatase (**d**) in buffer containing 0.2% (v/v) NP-40, 20 mM Tris-HCl, pH 9.0, 2 mM Ca^{2+}, 200 μM Zn^{2+}. (**e**) Kinetics of 2′3′-cGAMP and ATP hydrolysis by recombinant ENPP1. 1 nM ENPP1 was tested in the same buffer condition as **c** and **d**. Data are presented as mean ± s.e.

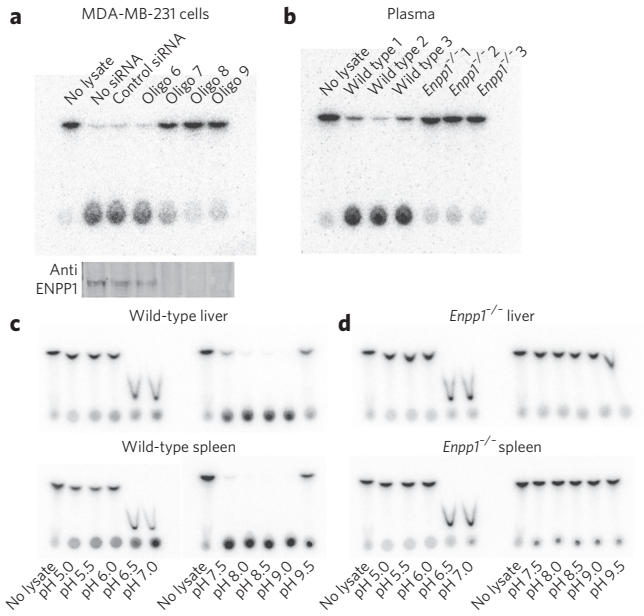

Figure 3 | ENPP1 is the dominant hydrolase activity for 2′3′-cGAMP. (**a**) Knockdown of ENPP1 in MDA-MB231 cells diminished hydrolase activity. Four siRNA oligos against ENPP1 with a control siRNA sequence against PDE12 were used. Four days after siRNA transfection, cells were lysed and assayed for activity (upper panel) and blotted for ENPP1 level (lower level). (**b**) Hydrolase activity in plasma from *Enpp1*$^{-/-}$ mice and their littermates. (**c**) Western blot characterization of *Enpp1*$^{-/-}$ mice. (**d**) Hydrolase activity in livers and spleens from *Enpp1*$^{-/-}$ mice and their littermates. Livers and spleens were minced and Dounce homogenized in lysis buffer containing 1% NP-40, 20 mM Tris-HCl, pH 7.5, and protease inhibitor cocktail. The assay was conducted in 0.2% NP-40, 20 mM Tris-HCl, 150 mM KCl, 2 mM Ca^{2+}, 2 mM Mg^{2+} and 200 μM Zn^{2+} at the indicated pH. NaOAc buffer was used for pH 5.0–6.0; PIPES buffer was used for pH 6.5 and 7.0; Tris-HCl buffer was used for pH 7.5–9.0, and borate buffer was used for pH 9.5. These buffer conditions were also used in liver and spleen extract studies. 2′3′-cGAMP runs at a lower R_f in PIPES buffer.

2′3′-cGAMP (K_{cat} = 4 s^{-1}, K_m = 15 μM; **Fig. 2e**). Thus, it is almost as active on 2′3′-cGAMP as it is on its known substrate, ATP.

ENPP1 is necessary for 2′3′-cGAMP hydrolysis

To test whether ENPP1 accounts for the dominant hydrolase activity in cells, we performed knockdown experiments in MDA-MB231 cells. Short interfering RNA (siRNA) oligos 7–9 against ENPP1 efficiently knocked down ENPP1 protein level and also marked reduced the hydrolase activity in the whole-cell lysate. Oligo 6 and the control siRNA against PDE12 did not affect ENPP1 protein level and also did not change the hydrolase activity. These results indicate that the dominant 2′3′-cGAMP hydrolase in this cell line is ENPP1 (**Fig. 3a**).

ENPP1 is an ecto-enzyme that can be shed or secreted into the serum[30]. Indeed, we detected high hydrolase activity in fetal bovine serum and human serum (**Supplementary Fig. 6**). Like the hydrolase activity in MDA-MB231 cells and in calf liver fractions, bovine and human serum hydrolase activity was also pH dependent, with peak activity at pH ~9.0, agreeing with the profile of ENPP1. To test whether ENPP1 accounts for most of the serum hydrolase activity, we tested plasma from *Enpp1*$^{-/-}$ mice. Although plasma from their wild-type littermates exhibited hydrolase activity, plasma from *Enpp1*$^{-/-}$ mice did not (**Fig. 3b**). Therefore, ENPP1 is the dominant hydrolase for 2′3′-cGAMP in mouse plasma. Given the pH profile and similar activity, we suspect that the same is true in human serum.

We next tested whether ENPP1 is the dominant 2′3′-cGAMP hydrolase in the liver and spleen. We chose to study the liver because it is the major site for drug metabolism and the spleen, owing to its important role in the immune system. We compared the hydrolase activity of livers and spleens from *Enpp1*$^{-/-}$ mice and their wild-type littermates. As we could have missed other hydrolases during our purification by using conditions not optimized for them, we surveyed a wide range of pH values and divalent ion concentrations. The migration profile of pure 2′3′-cGAMP at different pH conditions was generated to serve as the starting point (**Supplementary Fig. 5b**). At a point when extracts from wild-type counterparts had completely degraded 2′3′-cGAMP, extracts from ENPP1$^{-/-}$ livers and spleens showed undetectable levels of degradation (**Fig. 3c**). Together, our results demonstrate that ENPP1 is the dominant 2′3′-cGAMP hydrolase *in vivo*, at least in mice under our assay conditions.

Phosphothioate analogs are resistant to hydrolysis

Phosphothioate diester linkages are often resistant to hydrolysis by phosphodiesterases and nucleases and have been used to build important nonhydrolyzable ATP and GTP analogs. In addition to synthesizing a 3′-deoxy analog (**3**; 2′3′-cdGAMP), we enzymatically synthesized 2′3′-cGAMP analogs that used phosphothioate linkages in place of either the 3′-5′ (**4**; 2′3′-cG^{s}AMP) or the 2′-5′ (**5**; 2′3′-cGA^{s}MP) phosphodiester linkage or both (**6**; 2′3′-cG^{s}A^{s}MP; **Fig. 4a** and **Supplementary Figs. 7–9**). A higher enzyme concentration was required for 2′3′-cG^{s}A^{s}MP synthesis, and 2′3′-cG^{s}AMP synthesis was incomplete, indicating that cGAS is less efficient with when GTPαS is used as a starting material. Nevertheless, sufficient

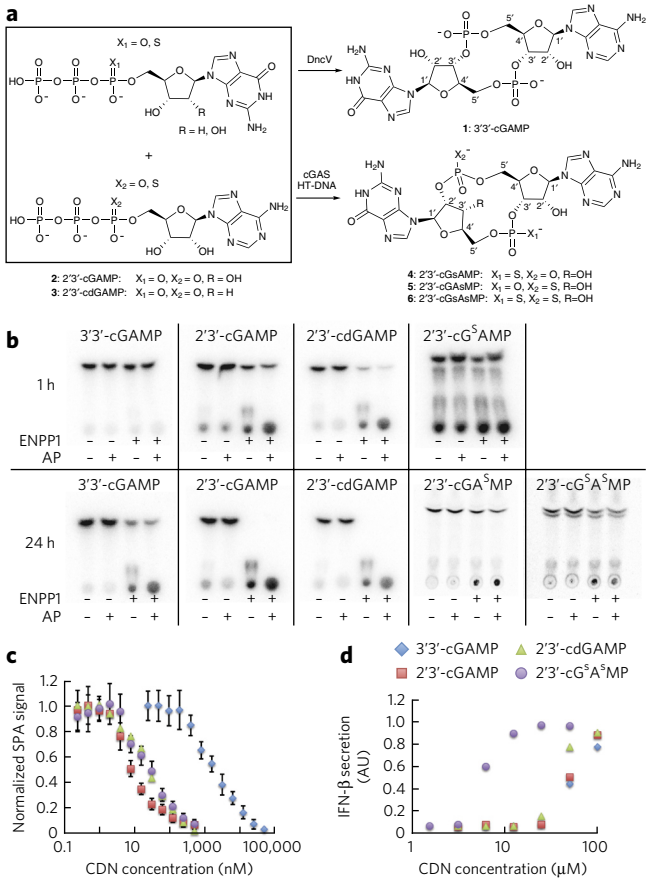

Figure 4 | Development of hydrolysis-resistant hSTING agonists. (**a**) Scheme of enzymatic synthesis of 3′3′-cGAMP and 2′3′-cGAMP analogs. For 3′3′-cGAMP, 50 nM of DncV was incubated with 1 mM ATP and 1 mM GTP in 1 ml buffer containing 20 mM Tris-HCl, pH 8.0, and 20 mM $MgCl_2$ for 3 h at room temperature. For 2′3′-cGAMP analogs, 1–10 μM mouse cGAS (residues 147–507) was incubated with 1 mM ATP, 1 mM GTP and 0.1 mg ml^{-1} DNA from herring testes (HT DNA) in 1 ml of the same buffer for 12 h at room temperature. (**b**) Hydrolysis reactions of ENPP1 (1 nM) with the analogs (10 μM) with or without the presence of alkaline phosphatase (AP). (**c**) SPA to measure the binding affinity of the analogs toward hSTING (residues 139–379). Biotinylated hSTING (100 nM) was immobilized onto 96-well streptavidin-coated SPA plates. Neat ^{35}S-labeled 2′3′-cGA^{S}MP (500 pM) was used as the probe. Data are presented as mean ± s.e.; $n = 3$. (**d**) IFN-β production in THP-1 cells stimulated with the analogs. THP-1 cells were incubated with the analogs at the indicated concentrations for 24 h. IFN-β in the medium was measured using a HEK-SEAP cell line. Representative data from biological triplicates are depicted. AU, arbitrary units.

2′3′-cG^{S}AMP was made to test its resistance to ENPP1 hydrolysis. We did not attempt to separate the diastereomers of these phosphothioate analogs but rather used them as mixtures, which are sufficient for proof of concept. We used the 3′-deoxy analog 2′3′-cdGAMP to evaluate the role of the 3′-hydroxyl group adjacent to the 2′-5′ phosphodiester bond.

We first tested the stability of these analogs in THP-1 cell lysates. Their relative stability is 2′3′-cG^{S}A^{S}MP > 3′3′-cGAMP >> 2′3′-cGAMP (**Supplementary Fig. 10a**). We then tested their stability toward 1 nM recombinant ENPP1, the concentration used in the kinetic analysis, either by itself or coupled with alkaline phosphatase. 2′3′-cGA^{S}MP and 2′3′-cG^{S}A^{S}MP were stable for at least 1 d, whereas all of the other 2′3′-cGAMP analogs exhibited half-lives of around 1 h in the presence of ENPP1 (**Fig. 4b**). 2′3′-cG^{S}A^{S}MP was able to inhibit 2′3′-cGAMP hydrolysis, suggesting it is capable of binding to ENPP1 and acting as a competitive inhibitor (**Supplementary Fig. 10b**). The increased stability of 2′-5′ phosphothioate analogs (at least 40 times more stable than 2′3′-cGAMP) suggest that cleavage of the 2′-5′ phosphodiester linkage is the first step and also the rate-limiting step catalyzed by ENPP1. This is consistent with our early observation that 3′3′-cGAMP, the bacterial CDN, is stable in the presence of mammalian cell lysate. Testing with pure ENPP1 confirmed that 3′3′-cGAMP is not a substrate (**Fig. 4b**). As 2′3′-cdGAMP is an ENPP substrate, the 3′-hydroxyl group is dispensable in the catalytic reaction (**Fig. 4b**). The relative stability of the analogs toward recombinant ENPP1 shares the same trend as whole-cell lysates. This structure-activity relationship study suggests that ENPP1 is the direct hydrolase of 2′3′-cGAMP rather than being indirectly involved in the regulation or activation of another hydrolase in the cell lysate.

2′3′-cG^{S}A^{S}MP has excellent STING agonist activity

We next tested the hSTING binding activity of 2′3′-cG^{S}A^{S}MP. We previously used fluorescence polarization and a fluorescent derivative of cyclic-di-GMP to measure the affinity of drugs for mSTING[7], but this approach failed with hSTING. Instead, we developed a scintillation proximity assay (SPA)-based competition binding assay (**Supplementary Fig. 11**). hSTING was biotinylated and immobilized onto streptavidin-coated SPA plates. ^{35}S-labeled 2′3′-cG^{S}A^{S}MP was used as a probe. The SPA signal increased with increasing amount of probe and reached saturation at 10 nM, with a K_d of ~5 nM. We used 500 pM of the probe in the competition assay, a concentration that yielded a high SPA signal but is well below the estimated K_d of the probe (K_{dprobe}). We then titrated in the analogs to measure their half-maximum inhibitory concentration (IC_{50}) values. According to the Cheng-Prusoff equation $K_d = IC_{50}/(1 + [probe]/K_{dprobe})$. Because $[probe] << K_{dprobe}$, the K_d values of the analogs are roughly equal to the measured IC_{50} values in this assay (**Fig. 4c**). We tested four CDN analogs using this assay. Consistent with previous reports that used calorimetric readouts[13], 3′3′-cGAMP is a much weaker ligand for hSTING ligand binding domain *in vitro* than 2′3′-cGAMP. The affinities of 23′-cG^{S}A^{S}MP and 2′3′-cdGAMP were comparable to that of 2′3′-cGAMP. Thus the nonhydrolyzable double phosphothioate analog is a good STING ligand.

We next tested whether the analogs can activate the STING pathway. All four analogs induced TBK1 phosphorylation within 2 h of drug addition in HEK 293 cells that express STING, suggesting direct activation (**Supplementary Fig. 12a**). We also tested HEK 293T cells, a subclone of the HEK 293 cells that do not express STING. 2′3′-cG^{S}A^{S}MP activated the TBK1-IRF3 axis in HEK 293 but not in HEK 293T cells, suggesting STING-dependent signaling (**Supplementary Fig. 12b**). To test the performance of these analogs in inducing IFN-β, we treated monocytic human THP-1 cells with the analogs for 24 h and measured secreted IFN-β using HEK-Blue IFN-α/β cells, a reporter cell line that responds to IFN-β by secreting alkaline phosphatase. The nonhydrolyzable 2′3′-cG^{S}A^{S}MP was the most potent analog at activating IFN-β (**Fig. 4d**), scoring with a half-maximum effective concentration (EC_{50}) approximately tenfold lower than that of natural 2′3′-cGAMP. To test whether its higher activity was due to increased biostability, we tested lung fibroblast cells from *Enpp1*$^{-/-}$ mice and their wild-type littermates. The hydrolysis-resistant 3′3′-cGAMP and 2′3′-cG^{S}A^{S}MP activated IFN-β to similar levels regardless of ENPP1 expression. In contrast, 2′3′-cGAMP is more active in *Enpp1*$^{-/-}$ cells, presumably owing to its prolonged half-life (**Fig. 5a–c** for female mice and **Supplementary Fig. 13** for male mice). The advantage of 2′3′-cG^{S}A^{S}MP over 2′3′-cGAMP is much smaller in *Enpp1*$^{-/-}$ cells, suggesting that biostability contributes substantially to its improved cellular activity.

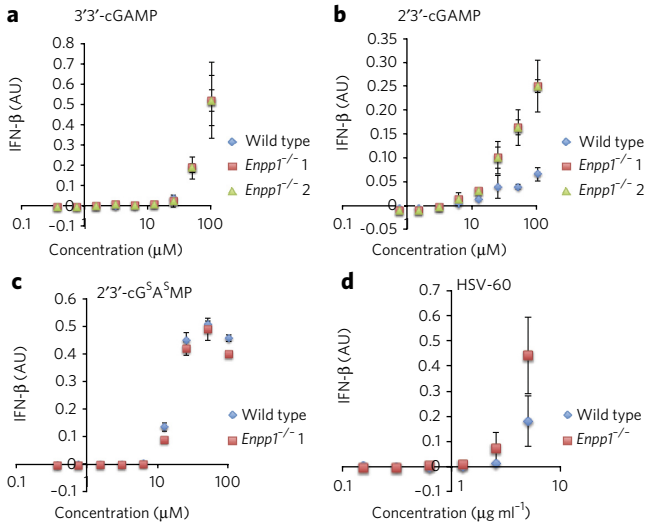

Figure 5 | ENPP1 dampens 2′3′-cGAMP signaling. Lung fibroblast cells from wild-type and *Enpp1*$^{-/-}$ female mice were incubated with 2′3′-cGAMP analogs (**a**–**c**) and HSV-60 (**d**) at the indicated concentrations for 24 h. IFN-β in the medium was measured using a B16-SEAP cell line. Data are presented as mean ± s.e.; $n = 3$. AU, arbitrary units.

Finally, to determine whether ENPP1 is important in shutting down the endogenous 2′3′-cGAMP pathway, we used HSV-60 (a 60-bp oligonucleotide containing viral DNA motifs) to activate this pathway. *Enpp1*$^{-/-}$ cells expressed notably more IFN-β in response to HSV-60 than wild-type cells, demonstrating its role as a negative regulator of the endogenous 2′3′-cGAMP pathway (**Fig. 5d**).

DISCUSSION

We identified a candidate 2′3′-cGAMP hydrolase by partially purifying this activity from a calf liver. Our purification procedures were remarkably short, and the final fraction is rather crude. However, MS analysis of this crude fraction was sufficient to generate the hypothesis that ENPP1 degrades 2′3′-cGAMP. We then used genetics to show that the dominant hydrolase activity for 2′3′-cGAMP in cells, tissues and blood is indeed ENPP1. Although we cannot rule out the possibility that other enzymes escaped our search because we did not find the optimum assay conditions for them, we showed that MDA-MB231 cells with ENPP1 knockdown as well as plasma, livers and spleens from *Enpp1*$^{-/-}$ mice all have negligible 2′3′-cGAMP hydrolase activity. The modern methods used in this study (early proteomic analysis of fractions and testing of mouse knockout tissues) show how proteins can be identified by activity-guided fractionation much more easily and more reliably now than in the past.

ENPP1-inactivating mutations and overexpression are known to cause a variety of disease phenotypes in humans and mice. This enzyme has rather broad substrate specificity, including ATP and NAD^{+}, and we have now shown that 2′3′-cGAMP is almost as good a substrate for recombinant ENPP1 as is ATP. This opens the question of which substrate (or substrates) are involved in ENPP1-related disease phenotypes. For example, ENPP1 is known to have important roles in bone mineralization. ENPP1-inactivating mutations are the cause of generalized arterial calcification of infancy, a deadly disease[31]. The current understanding is that ENPP1 hydrolyzes extracellular ATP to AMP and PP_i, and PP_i is a potent inhibitor of bone mineralization and calcification[32]. ENPP1 is also highly expressed in some breast tumors[33], and ENPP1 expression has been correlated with tamoxifen resistance[34]. Finally, a three-allele haplotype of ENPP1 is associated with obesity and higher risk of type 2 diabetes[35], although this linkage has not been found in all ethnic groups. The putative molecular mechanism for ENPP1's involvement in insulin signaling is that ENPP1 interacts with the insulin receptor directly to inhibit its phosphorylation and activation[36]. Studies of ENPP1 in mice also showed that high levels of ENPP1 suppress insulin signaling[37]. The enzymatic activity of ENPP1 is required for its inhibitory effect on insulin receptor signaling[38]. Our findings raise the question of whether 2′3′-cGAMP hydrolysis is responsible for any of these ENPP1-related diseases.

Our discovery of ENPP1 as 2′3′-cGAMP's major hydrolase sheds light on the regulation of the dsDNA-cGAS-STING innate immune pathway. This pathway has been shown to be downregulated by ULK-1 activation[39] and autophagy-mediated degradation of cGAS[40]. Loss of cytosolic 2′3′-cGAMP, either through hydrolysis or export, could provide another negative regulation mechanism, but we found no evidence for a 2′3′-cGAMP hydrolase activity in the cytosol from tissue culture cells, liver or spleen. Our data indicate that this new second messenger must be longer-lived than cAMP and cGMP in the cytosol, which are rapidly hydrolyzed by PDEs in the cytosol. This hypothesis is consistent with the observation that 2′3′-cGAMP can travel long distances through gap junctions[41].

ENPP1 activity is not found in the cytosol. Instead, it is found both on the basal lateral surface of the plasma membrane in hepatocytes and in the rough ER fraction from the liver. In the ER, its catalytic domain resides in the lumen[28], where there is high Ca^{2+} concentration necessary for its activity. Therefore, 2′3′-cGAMP must be transported across a membrane to be degraded, and it may have undiscovered activities once it has been transported. We do not know whether the ER lumen or the extracellular space is the major site for 2′3′-cGAMP degradation. There is no information on how permeable the ER membrane is to 2′3′-cGAMP. It is likely that there is an export mechanism for 2′3′-cGAMP as many other nucleotide derivatives (for example, ATP, NAD, cAMP and cGMP) have specific efflux pumps and have interesting extracellular biology. We (**Fig. 4d**) and others[9] have shown that this double-negatively charged small molecule functions when added to the medium without transfecting reagents, suggesting that a specific import mechanism may also exist. Given these results, we hypothesize that 2′3′-cGAMP may have interesting extracellular biology that is waiting to be explored (**Supplementary Fig. 14**).

Finally, our findings have major implications for the development of CDN-based hSTING agonist drugs. As 2′3′-cGAMP is the best ligand for hSTING (**Fig. 4c**)[13], it is at least in principle a good starting point for drug development. 2′3′-cGAMP is active when added to the outside of cells and has shown adjuvant activity in mice when injected intramuscularly[16], so it is apparently sufficiently stable to show some drug-like activity. Consistent with this, we find that it has a half-life in the range of minutes to 1 h in various biofluids and tissue lysates. Our bisphosphothioate analog 2′3′-cG^{S}A^{S}MP, which is ~40 times more resistant to ENPP1 hydrolysis, is expected to last much longer in biofluids and showed ~10 times higher cell-based activity in culture (**Fig. 4d**). This higher activity was not due to tighter STING binding (**Fig. 4c**) and is likely to be due to increased biostability (**Fig. 5**). We propose that 2′3′-cG^{S}A^{S}MP will be a useful tool compound in further exploring the biology and metabolism of 2′3′-cGAMP and for testing whether CDN analogs deserve further development as clinical candidates.

Received 20 July 2014; accepted 28 August 2014; published online 26 October 2014; corrected after print 29 January 2015

METHODS

Methods and any associated references are available in the online version of the paper.

References

1. Duthie, M.S., Windish, H.P., Fox, C.B. & Reed, S.G. Use of defined TLR ligands as adjuvants within human vaccines. *Immunol. Rev.* **239**, 178–196 (2011).

2. Coffman, R.L., Sher, A. & Seder, R.A. Vaccine adjuvants: putting innate immunity to work. *Immunity* **33**, 492–503 (2010).
3. Hemmi, H. *et al.* Small anti-viral compounds activate immune cells via the TLR7 MyD88-dependent signaling pathway. *Nat. Immunol.* **3**, 196–200 (2002).
4. Ishikawa, H. & Barber, G.N. STING is an endoplasmic reticulum adaptor that facilitates innate immune signalling. *Nature* **455**, 674–678 (2008).
5. Zhong, B. *et al.* The adaptor protein MITA links virus-sensing receptors to IRF3 transcription factor activation. *Immunity* **29**, 538–550 (2008).
6. Wu, J. *et al.* Cyclic GMP-AMP is an endogenous second messenger in innate immune signaling by cytosolic DNA. *Science* **339**, 826–830 (2013).
7. Kim, S. *et al.* Anticancer flavonoids are mouse-selective STING agonists. *ACS Chem. Biol.* **8**, 1396–1401 (2013).
8. Conlon, J. *et al.* Mouse, but not human STING, binds and signals in response to the vascular disrupting agent 5,6-dimethylxanthenone-4-acetic acid. *J. Immunol.* **190**, 5216–5225 (2013).
9. Gao, P. *et al.* Structure-function analysis of STING activation by c[G(2′,5′) pA(3′,5′)p] and targeting by antiviral DMXAA. *Cell* **154**, 748–762 (2013).
10. Burdette, D.L. *et al.* STING is a direct innate immune sensor of cyclic di-GMP. *Nature* **478**, 515–518 (2011).
11. Tanaka, Y. & Chen, Z.J. STING specifies IRF3 phosphorylation by TBK1 in the cytosolic DNA signaling pathway. *Sci. Signal.* **5**, ra20 (2012).
12. Davies, B.W., Bogard, R.W., Young, T.S. & Mekalanos, J.J. Coordinated regulation of accessory genetic elements produces cyclic di-nucleotides for *V. cholerae* virulence. *Cell* **149**, 358–370 (2012).
13. Zhang, X. *et al.* Cyclic GMP-AMP containing mixed phosphodiester linkages is an endogenous high-affinity ligand for STING. *Mol. Cell* **51**, 226–235 (2013).
14. Ablasser, A. *et al.* cGAS produces a 2′-5′-linked cyclic dinucleotide second messenger that activates STING. *Nature* **498**, 380–384 (2013).
15. Diner, E.J. *et al.* The innate immune DNA sensor cGAS produces a noncanonical cyclic dinucleotide that activates human STING. *Cell Rep.* **3**, 1355–1361 (2013).
16. Li, X.D. *et al.* Pivotal roles of cGAS-cGAMP signaling in antiviral defense and immune adjuvant effects. *Science* **341**, 1390–1394 (2013).
17. Bender, A.T. & Beavo, J.A. Cyclic nucleotide phosphodiesterases: molecular regulation to clinical use. *Pharmacol. Rev.* **58**, 488–520 (2006).
18. Maurice, D.H. *et al.* Advances in targeting cyclic nucleotide phosphodiesterases. *Nat. Rev. Drug Discov.* **13**, 290–314 (2014).
19. Wielinga, P.R. *et al.* Characterization of the MRP4- and MRP5-mediated transport of cyclic nucleotides from intact cells. *J. Biol. Chem.* **278**, 17664–17671 (2003).
20. Jedlitschky, G., Burchell, B. & Keppler, D. The multidrug resistance protein 5 functions as an ATP-dependent export pump for cyclic nucleotides. *J. Biol. Chem.* **275**, 30069–30074 (2000).
21. Guo, Y. *et al.* MRP8, ATP-binding cassette C11 (ABCC11), is a cyclic nucleotide efflux pump and a resistance factor for fluoropyrimidines 2′,3′-dideoxycytidine and 9′-(2′-phosphonylmethoxyethyl)adenine. *J. Biol. Chem.* **278**, 29509–29514 (2003).
22. Gao, P. *et al.* Cyclic [G(2′,5′)pA(3′,5′)p] is the metazoan second messenger produced by DNA-activated cyclic GMP-AMP synthase. *Cell* **153**, 1094–1107 (2013).
23. Sun, L., Wu, J., Du, F., Chen, X. & Chen, Z.J. Cyclic GMP-AMP synthase is a cytosolic DNA sensor that activates the type I interferon pathway. *Science* **339**, 786–791 (2013).
24. Kubota, K. *et al.* Identification of 2′-phosphodiesterase, which plays a role in the 2–5A system regulated by interferon. *J. Biol. Chem.* **279**, 37832–37841 (2004).
25. Poulsen, J.B. *et al.* Human 2′-phosphodiesterase localizes to the mitochondrial matrix with a putative function in mitochondrial RNA turnover. *Nucleic Acids Res.* **39**, 3754–3770 (2011).
26. Goding, J.W. *et al.* Ecto-phosphodiesterase/pyrophosphatase of lymphocytes and non-lymphoid cells: structure and function of the PC-1 family. *Immunol. Rev.* **161**, 11–26 (1998).
27. Bollen, M., Gijsbers, R., Ceulemans, H., Stalmans, W. & Stefan, C. Nucleotide pyrophosphatases/phosphodiesterases on the move. *Crit. Rev. Biochem. Mol. Biol.* **35**, 393–432 (2000).
28. Bischoff, E., Tran-Thi, T.A. & Decker, K.F. Nucleotide pyrophosphatase of rat liver. A comparative study on the enzymes solubilized and purified from plasma membrane and endoplasmic reticulum. *Eur. J. Biochem.* **51**, 353–361 (1975).
29. Kato, K. *et al.* Crystal structure of Enpp1, an extracellular glycoprotein involved in bone mineralization and insulin signaling. *Proc. Natl. Acad. Sci. USA* **109**, 16876–16881 (2012).
30. Belli, S.I., van Driel, I.R. & Goding, J.W. Identification and characterization of a soluble form of the plasma cell membrane glycoprotein PC-1 (5′-nucleotide phosphodiesterase). *Eur. J. Biochem.* **217**, 421–428 (1993).
31. Rutsch, F. *et al.* PC-1 nucleoside triphosphate pyrophosphohydrolase deficiency in idiopathic infantile arterial calcification. *Am. J. Pathol.* **158**, 543–554 (2001).
32. Hessle, L. *et al.* Tissue-nonspecific alkaline phosphatase and plasma cell membrane glycoprotein-1 are central antagonistic regulators of bone mineralization. *Proc. Natl. Acad. Sci. USA* **99**, 9445–9449 (2002).
33. Lau, W.M. *et al.* Enpp1: A potential facilitator of breast cancer bone metastasis. *PLoS ONE* **8**, e66752 (2013).
34. Umar, A. *et al.* Identification of a putative protein profile associated with tamoxifen therapy resistance in breast cancer. *Mol. Cell. Proteomics* **8**, 1278–1294 (2009).
35. Meyre, D. *et al.* Variants of ENPP1 are associated with childhood and adult obesity and increase the risk of glucose intolerance and type 2 diabetes. *Nat. Genet.* **37**, 863–867 (2005).
36. Rey, D. *et al.* Amerindians show no association of PC-1 gene Gln121 allele and obesity: a thrifty gene population genetics. *Mol. Biol. Rep.* **39**, 7687–7693 (2012).
37. Maddux, B.A. *et al.* Membrane glycoprotein PC-1 and insulin resistance in non-insulin-dependent diabetes mellitus. *Nature* **373**, 448–451 (1995).
38. Chin, C.N. *et al.* Evidence that inhibition of insulin receptor signaling activity by PC-1/ENPP1 is dependent on its enzyme activity. *Eur. J. Pharmacol.* **606**, 17–24 (2009).
39. Konno, H., Konno, K. & Barber, G.N. Cyclic dinucleotides trigger ULK1 (ATG1) phosphorylation of STING to prevent sustained innate immune signaling. *Cell* **155**, 688–698 (2013).
40. Liang, Q. *et al.* Crosstalk between the cGAS DNA sensor and Beclin-1 autophagy protein shapes innate antimicrobial immune responses. *Cell Host Microbe* **15**, 228–238 (2014).
41. Ablasser, A. *et al.* Cell intrinsic immunity spreads to bystander cells via the intercellular transfer of cGAMP. *Nature* **503**, 530–534 (2013).

Acknowledgments

We thank P. Koch, P. Choi, K. Krukenberg, A. Groen, M. Loose, S. Kim and S. Gruver for helpful discussions. We thank R. Jiang for help with data analysis. We thank K. Chu for providing mouse livers. We thank S. Walker for sharing the MicroBeta plate reader and C. Fan for technical assistance. We thank J.J. Mekalanos for providing the DncV expression plasmid and T. Bernhard (both from Harvard Medical School) for providing the pTB146 plasmid. We thank G. Heffron and C. Sheahan for assistance with the NMR data collection and analysis. We thank R. Ward for help with manuscript preparation. This research was supported by the National Cancer Institute (CA139980, AR53102, AI050872 and 1K99AI108793-01). L. Li thanks the Jane Coffin Childs Fund for her postdoctoral fellowship.

Author contributions

L.L. and T.J.M. developed the hypothesis and designed the study. L.L., Q.Y., P.K. and Z.M. conducted the experiments. All authors interpreted and discussed the results. J.L.M. advised P.K., and H.W. advised Q.Y. Both J.L.M. and H.W. funded part of the research. L.L. and T.J.M. wrote the manuscript.

Competing financial interests

The authors declare no competing financial interests.

Additional information

Supplementary information and chemical compound information is available in the online version of the paper. Reprints and permissions information is available online at http://www.nature.com/reprints/index.html. Correspondence and requests for materials should be addressed to L.L.

ONLINE METHODS

Reagents, antibodies and cell lines. [α-^{32}P]ATP (3,000 Ci/mmol, 10 mCi/ml, 250 μCi) and [^{35}S]ATPαS (1,250 Ci/mmol, 12.5 mCi/ml, 250 μCi) were purchased from PerkinElmer. Adenosine-5′-*O*-(1-thiotriphosphate), guanosine-5′-*O*-(1-thiotriphosphate) and 3′-deoxyguanosine-5′-triphosphate were purchased from Trilink Biotechnologies. ATP, GTP and herring testes DNA were purchased from Sigma-Aldrich. EZ-Link Sulfo-NHS-LC-Biotin was purchased from Pierce (21335). Set of Four ON-TARGETplus PDE12 siRNA (LQ-017946-01-0002) and Set of Four ON-TARGETplus ENPP1 siRNA (LQ-003809-00-0002) were purchased from Dharmacon. Anti-PDE12 antibody (ab87738, 1:1,000 dilution) was from Abcam. Anti-ENPP1 antibody (no. 2061) was from Cell Signaling. Rabbit polyclonal antibodies against TBK, pTBK (S172, 1:1,000 dilution), pIRF3 (S396, 1:1,000 dilution) and STING were purchased from Cell Signaling Technology. HSV-60/LyoVec, HEK-Blue IFN-α/β cells and B16-Blue IFN-α/β cells were purchased from Invivogen. Recombinant ENPP1 was purchased from R&D Systems (6136-EN-010). Collagenase D was from Roche, and trypsin was from Sigma.

Cell culture and siRNA transfection. L929 and HEK-Blue IFN-α/β cells were maintained in DMEM (Cellgro) supplemented with 10% FBS (GIBCO) (v/v) and 1% penicillin-streptomycin (Cellgro). THP-1 cells were grown in RPMI (Cellgro) supplemented with 10% FBS, 0.1% β-mercaptoethanol (GIBCO) and 1% penicillin-streptomycin. MDA-MB231 cells were grown in RPMI supplemented with 10% FBS and 1% penicillin-streptomycin.

Expression and purification of recombinant proteins. All procedures involving proteins and cell lysates were conducted at 4 °C unless stated otherwise.

DncV expression plasmid was a generous gift from J.J. Mekalanos at Harvard Medical School, and the protein was produced using the established protocol[12].

The DNA sequence encoding mouse cGAS (residues 147–507) was amplified from the cDNA library generated from L929 cells using the primer pair: mcGAS-147-FWD TATTGAGGCTCACAGAGAACAGATTGGTGGT CCGGACAAGCTAAAGAAGGTGCT and mcGAS-REV GGATCCCCTTCCT GCAGTCACCCGGGCTCGAG TCAAAGCTTGTCAAAAATTGGAAA. The PCR product was inserted into the SapI and XhoI sites of pTB146 (a generous gift from T. Bernhard at Harvard Medical School) using isothermal assembly. His-SUMO–tagged mcGAS (residues 147–507) was expressed in Rosetta Competent Cells. Cells were grown in LB medium with ampicillin (100 ng/ml) and were induced with 0.5 mM IPTG when the OD reached 1 and were allowed to grow overnight at 16 °C. Cells were pelleted and lysed. The cell extract was then cleared by ultracentrifugation at 45,000 r.p.m. for 1 h. The cleared supernatant was incubated with Ni-NTA beads (4 ml of beads per liter of bacteria culture). Ni beads were washed with 20 mM imidazole in PBS, and protein was eluted with step concentrations of 50 mM to 500 mM imidazole in PBS. Fractions containing his-SUMO-mcGAS were pooled, concentrated and dialyzed against PBS. The protein was further purified by size-exclusion chromatography in running buffer containing z20 mM Tris HCl (pH 8.0), 150 mM NaCl and 2 mM Mg^{2+}. Fractions containing mcGAS (residues 147–507) were pooled, concentrated and snap frozen for future use.

DNA encoding full-length human PDE12 was cloned into a modified version of pDB-His-MBP vector. The protein was expressed in *Escherichia coli* BL21 DE3 RIPL Codon-Plus cells. *E. coli* cells were induced by 0.4 mM IPTG when cell density reached 0.6 and were grown at 20 °C overnight. Cells were pelleted and lysed. After centrifugation and removal of cell debris, the supernatant was incubated with Ni-NTA beads. Ni beads were washed extensively, and protein was eluted in lysis buffer with 300 mM imidazole. After cleavage by PreScission protease, the N-terminal His_6-MBP was removed by incubation with Ni-NTA beads. PDE12 protein in the flow-through fractions was further purified by size-exclusion chromatography.

Enzymatic synthesis of 3′3′-cGAMP and 2′2′-cGAMP analogs. For 3′3′-cGAMP, 50 nM of DncV was incubated with 1 mM ATP and 1 mM GTP in 1 ml buffer containing 20 mM Tris-HCl, pH 8.0, and 20 mM $MgCl_2$ at room temperature for 3 h. For 2′3′-cGAMP analogs, 1–10 μM mouse cGAS (residues 147–507) was incubated with 1 mM ATP, 1 mM GTP and 0.1 mg/ml HT-DNA in 1 ml of the same buffer for 12 h at room temperature. The reaction mixtures were then heated at 95 °C for 3 min and filtered through a 3-kDa filter. The product was purified using a silica plug with 5 mM NH_4HCO_3/15% H_2O/85% EtOH as the mobile phase. To make the ^{32}P- and ^{35}S-labeled CDNs for degradation assays, 10 μCi [α-^{32}P]ATP or [^{35}S]ATPαS were mixed in with the cold starting materials. The reaction mixture was filtered through a 3-kDa filter and used without further purification. To synthesize neat ^{35}S-labeled 2′3′-cGA^{s}MP for the SPA assay, 250 μCi [^{35}S]ATPαS and 100 μM cold GTP were used as the starting material in 100 μl buffer. The product was purified using a silica plug with 5 mM NH_4HCO_3/15% H_2O/85% EtOH as the mobile phase.

Mice. Generation and characterization has been reported previously for *Enpp1*$^{-/-}$ mice[42,43]. Genotyping was performed with PCR protocols on genomic DNA. Anesthesia was given intraperitoneally with 2,2,2-tribromoethanol (Avertin). Blood was collected by cardiac puncture into lithium heparin tubes; tissues were frozen immediately in liquid nitrogen. The Institutional Animal Care and Use Committee (IACUC) approved all animal procedures.

Preparation of cell and tissue extracts. To determine whether THP-1 cells, L929 cells and MDA-MB231 cells have hydrolase activity for 2′3′-cGAMP, the whole-cell lysate was generated using lysis buffer containing 10 mM Tris-HCl, pH 7.5,150 mM NaCl, 1% NP-40, 1.5 mM MgCl, 2 mM DTT and protease inhibitor tablet (Roche) at 1 ml for 100 million cells. To determine the subcellular location of the hydrolase (or hydrolases), cells were lysed by Dounce homogenization in either a mitochondria-friendly buffer (10 mM Tris-MOPS (pH 7.4), 10 mM EDTA/Tris, 200 mM sucrose) or a hypotonic buffer (10 mM Tris-HCl, pH 7.5, 10 mM KCl, 1.5 mM $MgCl_2$, 2 mM DTT, protease inhibitor tablet). The homogenate was then subjected to centrifugation at 600*g* and 7,000*g*.

To prepare whole-cell lysate, liver and spleen extracts to test the role of ENPP1, the cells and tissue samples were minced and Dounce homogenized in detergent containing buffer consisting of 20 mM Tris-HCl, pH 7.5, 1% NP-40 and a protease inhibitor tablet. The lysate were tested without centrifugation clearance at different pH values in the presence of 150 mM KCl, 2 mM $MgCl_2$, 2 mM $CaCl_2$ and 200 μM $ZnCl_2$. 100 mM NaOAc buffer was used for pH 5.0–6.0; 100 mM PIPES buffer was used for pH 6.5 and 7.0; 100 mM Tris-HCl buffer was used for pH 7.5–9.0; and 100 mM borate buffer was used pH 9.5.

TLC analysis of CDN synthesis and degradation. This protocol was modified from established protocol[22]. Reaction solution (1.5 μl) was spotted onto TLC plates (HPTLC silica gel, 60 Å pores, F_{254}, 1055480001; MERCK Millipore), and the nucleotides were separated with 5 mM NH_4HCO_3/15% H_2O/85% EtOH as the mobile phase at 25 °C for 30 min. The plates were visualized by UV (254 nm) or by autoradiography. Images were processed using Adobe Photoshop and Illustrator CS6.

Partial purification of ENPP1 from a calf liver. The calf liver was homogenized in buffer A, consisting of 10 mM Tris-MOPS (pH 7.4), 10 mM EDTA/Tris and 200 mM sucrose. For subcellular fractionation, the homogenate was centrifuged at 600*g* for 20 min to remove cell debris and nuclei. The supernatant was centrifuged at 7,000*g* for 20 min to precipitate mitochondria and other heavy organelles. The pellet was resuspended in 200 ml buffer A and centrifuged at 7,000*g* for 20 min. Both the supernatant and the pellet were analyzed for activity in reaction buffer containing 20 mM Tris-HCl, pH 7.5, 1% NP-40 and 1 mM $CaCl_2$. The supernatant was where the activity resided, so it was then centrifuged at 45,000*g* for 1 h, and all the activity was precipitated. The pellet was extracted using the detergent-containing reaction buffer and cleared by centrifuging at 45,000*g* for 1 h. The supernatant was subjected to anion exchange fractionation using a 5-ml HiTrap Q column followed by size exclusion fractionation using a Superose 6 column. Fraction 26 contained high activity but had an undetectable amount of protein, as shown by SDS-PAGE gel and Coomassie blue staining. The entire lane was subjected to MS analysis at the Taplin Mass Spectrometry Facility at Harvard Medical School as a standard service, identifying 377 proteins (**Supplementary Data Set**). ENPP1, which ranked no. 17 on the list, was the top candidate because it is the only phosphodiesterase on the list judging by their annotations.

SPA. Wild-type hSTING (230G/232R, residues 139–379) was prepared as described before[7]. The protein was dialyzed in PBS for 3 h to remove trace amount of Tris-HCl that would react with the labeling reagent. The protein was labeled at 300 μM with 3 equivalents of EZ-Link Sulfo-NHS-LC-Biotin at room temperature for 30 min. Another 3 equivalents of the labeling reagent were added and allowed to react for another 30 min. Bovine serum albumin

was labeled using the same protocol as a control. The proteins were then dialyzed in PBS to remove free biotin. To immobilize the proteins onto 96-well streptavidin-coated SPA plates (PerkinElmer 1450-551), biotinylated hSTING and the BSA control (100 nM) were incubated on the plates for 30 min. The plates were then washed three times with PBS. To decide the K_d of the probe, serial dilutions of neat ^{35}S-labeled 2′3′-cGA^{s}MP (0.01 nM to 20 nM) were incubated with immobilized protein for 30 min. The probe was then aspirated and read on a 1450 MicroBeta TriLux for 3 min. For the competition assay, 500 pM ^{35}S-labeled 2′3′-cGA^{s}MP in PBS was used to make the serial dilutions of the CDNs. The cold CDN and probe mixtures were incubated with the protein plates for 30 min. The wells were aspirated dry and read on the MicroBeta plate reader.

SEAP assay. HEK-Blue IFN-α/β cells were used to measure IFN-α/β produced by THP-1 cells. We followed the manufacturer-recommended protocols. Briefly, 24 h after drug treatment, conditioned media were collected and added to the HEK-Blue reporter cells. After 18 h, SEAP activity was measured using a Victor plate reader (PerkinElmer). B16-Blue IFN-α/β cells were used to measure IFN-α/β produced by mouse lung fibroblast cells. The assay protocol is the same as that for HEK-Blue IFN-α/β cells.

Isolation of lung fibroblast cells. Lungs from each mouse were minced in a Petri dish and digested in 5 ml of DMEM with 0.1% collagenase D and 0.2% trypsin at 37 °C for 1 h. The mixture was pipetted up and down every 10 min. Disassociated cells were washed twice in DMEM and pelleted at 1,200*g*, 4 °C for 10 min to remove enzymes. Cells were resuspended in complete medium (DMEM, 10% FBS, Penstrep and Fungizone) and seeded in a 10-cm dish. The fibroblast cells attached in 1 h, and the rest of the cells were washed away by replacing the medium.

42. Sali,, A.F.J.M., Terkeltaub, R. & Goding, J.W. in *Ecto-ATPases and Related Ectonucleotidases* (eds. Vanduffel, L. & Lemmens, R.) 267–282 (Shaker Publishing BV, Maastricht, the Netherlands, 1999).
43. Narisawa, S. *et al.* Novel inhibitors of alkaline phosphatase suppress vascular smooth muscle cell calcification. *J. Bone Miner. Res.* **22**, 1700–1710 (2007).

doi:10.1038/nchembio.1661

CORRIGENDUM

Hydrolysis of 2′3′-cGAMP by ENPP1 and design of nonhydrolyzable analogs

Lingyin Li, Qian Yin, Pia Kuss, Zoltan Maliga, José L Millán, Hao Wu & Timothy J Mitchison

Nat. Chem. Biol. **10**, 1043–1048 (2014); published online 26 October 2014; corrected after print 29 January 2015

In the version of this article initially published, the chemical structures of the two cyclic dinucleotides in Figure 4a were incorrect at the triphosphate group, with each of the phosphates shown as containing two extra hydrogen atoms. The error has been corrected in the HTML and PDF versions of the article.